CHALMERS

Numerical Studies of Effective Diffusivity in Fibrous Porous Media

Master of Science's Thesis in Applied Physics

HÅKAN CARLSSON

Department of Applied Physics
Division of Chemical Physics
CHALMERS UNIVERSITY OF TECHNOLOGY
Gothenburg, Sweden 2013
Master's Thesis 2013

Numerical Studies of Effective Diffusivity in Fibrous Porous Media

HÅKAN CARLSSON

Department of Applied Physics
Division of Chemical Physics
Chalmers University of Technology
Göteborg, Sweden 2013

Numerical studies of effective diffusivity in fibrous porous media

HÅKAN CARLSSON

Cover illustration: *Example of a three dimensional random walk simulation in fibrous porous media. The structure consists of discretized one dimensional fibres aligned perpendicularly to the viewing plane, where the trajectories of the walkers are projected as green lines. The red and yellow crosses represent a walker-fibre and walker-walker collision, respectively. If the mean free path of the walker is greater then the mean distance between fibres, the number of walker-fibre collisions will be greater than the walker-walker collisions, as shown in the figure.*

Numerical studies of effective diffusivity in fibrous porous media

HÅKAN CARLSSON
Department of Applied Physics
Division of Chemical Physics
Chalmers University of Technology
Göteborg, Sweden 2013

Abstract

Current modelling of effective diffusivity in the Gas Diffusion Layer (GDL) of the Polymer Exchange Membrane Fuel Cell (PEMFC), often relies on semi-empirical equations with limited accuracy. In particular, there is a need to develop models incorporating the microscopic structure of the porous GDL when performing flow simulations. The objective of this thesis is to construct a simulation program based on random walk methodology, to calculate the effective diffusivity of realistic scanned porous media. This approach has the advantage of not making any structural assumptions about the material other than the resolution of the scanned images, and various aspects of the material can thus be investigated. The simulation program is validated with literature data of the effective diffusivity of continuous random fibres, defined by point and direction. This present study however is performing random walks in uniform grids where the voxels are either void or solid. A qualitative simulation program was developed and the validation results showed an relative error of 50% compared to the Bosanquet formula, thus more work needs to be done.

Keywords: PEMFC, GDL, diffusion, porous media, random walk, Monte Carlo simulations.

Acknowledgements

This thesis would not have been possible without the support of many people. The author wishes to express his gratitude to both his supervisors, Prof. Dr. Aimy Bazylak and Prof. Dr. Henrik Grönbeck who were abundantly helpful and provided significant support.

Deepest gratitude are also due to Matias Nordin, without whose invaluable assistance this study would not have been successful.

Special thanks also to Dr. Ramses Van Zon and Prof. Dr. Stu G. Whittington for many insightful discussions.

Håkan, Göteborg January 24, 2013

Contents

1

Introduction

Recent climate changes urges new methods in energy usage. For instance, the current combustion engine uses fossil fuels, and transform it into house gases. A promising candidate to make the necessary shift from the current carbon based technology are fuel cells, and the significant change they impose is energy conversion. In particular, hydrogen can be produced from renewable energy sources and when used in fuel cells, the main reaction product is water.

A number of different types of fuel cells have emerged with their different disadvantages and advantages depending on the application. The Solid Oxide Fuel Cell (SOFC) has a long durability, but it operates at high temperatures ($\sim 1000\,^\circ$C), which put requirements on the material. The Polymer Exchange Membrane Fuel Cell (PEMFC) is, however, a promising candidate for many types of applications due to its low temperature, low weight, compactness and sustainability for discontinuous operation [1]. These properties make the PEMFC suitable for portable power supply, transportation and stationary power systems [1]. For instance, the PEMFC can work as an Auxiliary Power Unit (APU) in trucks or sailing yachts, or a small-scale PEMFC can supply energy to a laptop.

There is, however, a number of challenges to overcome to render a full-scale commercialisation of the PEMFC possible. To address these problems, fuel cell developers are trying to optimize the design of the PEMFC by computer simulations of the entire system [2]. These simulations, however, describe the macroscopic behaviour of the system, relying on models for the microscopic structure of the components. Without accurate models for capturing the statistical properties of the microscopic behaviour, the results of macroscopic modelling will inevitably be imprecise. One such critical component for the performance of the PEMFC, is the Gas Diffusion Layer (GDL). It is a porous membrane where transport of gas reactants and waste products to and from the catalyst sites occur, and it is typically built up from fibres with diameters in the micrometer regime. Due to it's influence of the flow rates of reactants and products, it is a major component
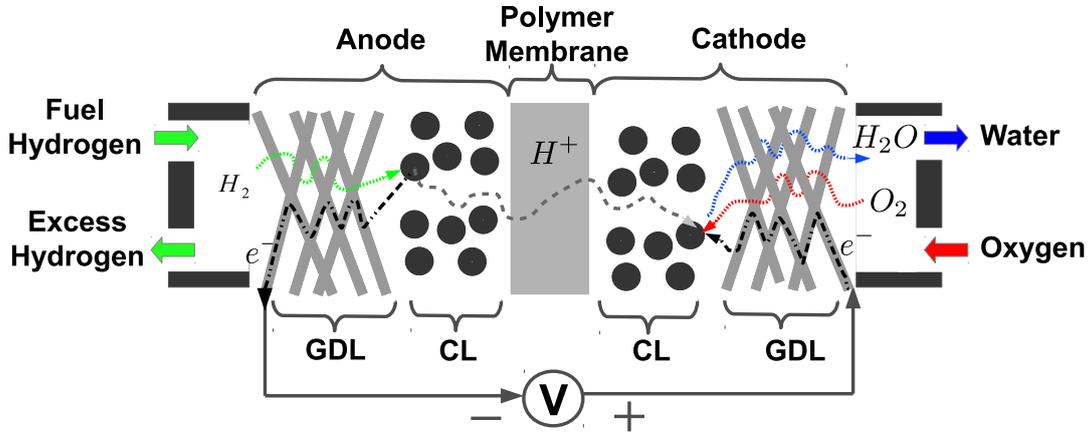
Figure 1.1: Schematic figure of a PEMFC.

for the overall performance of the PEMFC.

One transport phenomenon in the GDL is diffusion, which is described quantitatively by the effective diffusivity. Current full-scale PEMFC modelling, relies mainly on inaccurate theories describing effective diffusivity in porous media [3]. These models for porous media are not sufficiently accurate for fuel cell modelling, and there is an discrepancy between theory and experiments [4]. Commonly, models describing diffusion in porous media are based on structural assumptions of the material, followed by regression of data retrieved from numerical simulations or analytical studies. However, porous media has in general a significant complex structure, which render it difficult to model.

The objective of this study is to expand the work of Tomadakis [5], who investigated the diffusivity properties of geometric fibres modelled as cylinders, and write a simulation program adapted for scanned porous material obtained from 3D imaging experiments. Validation will be the major goal, obtaining the same results as Tomadakis for similar domains. With this program the effective diffusivity can be obtained from realistic porous domains not restricted to geometric fibres, but for arbitrary domains.

1.1 Fuel Cells

Fuel cells convert chemical energy to electrical energy without the efficiency penalty of Carnot process. A combustive engine, driven the thermodynamic cycle will not be as efficient as the fuel cell which take advantage of electromechanical and chemical processes.

A schematic of the Polymer Exchange Membrane Fuel Cell is shown in Fig. 1.1. Hydrogen splits into electrons and protons at the anode. The electrons forms an electrical current to drive a load, for instance an electrical motor, and the protons are conducted through a polymer membrane. Finally, protons and electrons forms water after reduction

reaction with oxygen at the cathode. The chemical reactions are thus,

$$\textbf{Anode:} \qquad H_2 \qquad \rightarrow 2H^+ + 2e \qquad (1.1a)$$

$$\textbf{Cathode:} \quad 1/2O_2 + 2H^+ + 2e^- \quad \rightarrow H_2O \qquad (1.1b)$$

$$\textbf{Overall:} \qquad H_2 + 1/2O_2 \qquad \rightarrow H_2O \qquad (1.1c)$$
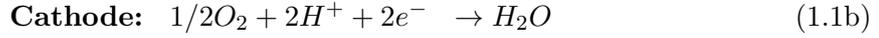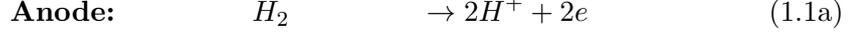
As mentioned, a critical part of the fuel cell is the Gas Diffusion Layer (GDL). The main purpose of the GDL is to provide mechanical stability for the polymer membrane and the catalyst layer (CL). Therefore oxygen has to be diffused through the GDL to the CL, where the reduction reaction occurs. The CL contains platinum, to enable and increase the rate of reactions. Consequently, the power output is proportional to the reaction rate [6], which is then dependent on the diffusivity of oxygen through the GDL.

Today, the challenges impeding the PEMFC large scale commercialization are: prolong membrane lifetime, increase the power density and reduce platinum loading [7]. One solution to the two latter, is to increase mass transfer rates in the GDL. It would give higher current densities, higher reactant concentrations in the CL and less platinum is required. Hence, there is a need to improve the understanding of the transport phenomena, specifically the diffusion, of the GDL to increase the mass transfer rate. As with any type of product development, a good methodology is to first evaluate the design numerically, and then verify by experiments.

1.1.1 Gas Diffusion Layer

The GDL is a porous medium, consisting of different types of materials (e.g. carbon fibres) organised in different structures (e.g. woven, cloth). A Scanning Electron Microscope (SEM) picture of a GDL shown in Fig. 1.2, depicts one example of the microscopic structure. As can be seen, the GDL consists of a complex network fibres and binders. The structure of the GDL allows the gases to spread out as they diffuse to catalyst layer, in order to maximize the contact surface area between the gases and the catalyst layer.

In addition to diffuse reactant gases, the GDL has to remove the water produced from the reaction at the cathode [6]. If water production rate is greater than the water removal rate, water will accumulate in the GDL and reduce the pore size of the porous media, and consequently decrease the rate of oxygen diffusion. The solution for water management is to coat the fibres with a hydrophobic layer, and consequently the complexity of the structure [9] is increased.

Given the complex structure of the GDL, many models treat the GDL microstructure as a bulk material [10, 11, 12], when performing macroscopic simulations of the fuel cell system. To obtain the effective diffusivity D_{eff}, a formation factor f is introduced [6],

$$D_{eff} = f \cdot D_0, \qquad (1.2)$$

and can be interpreted as a correction factor to the reference diffusivity D_0. The form factor f contains all the structural properties of the material influencing the diffusivity,
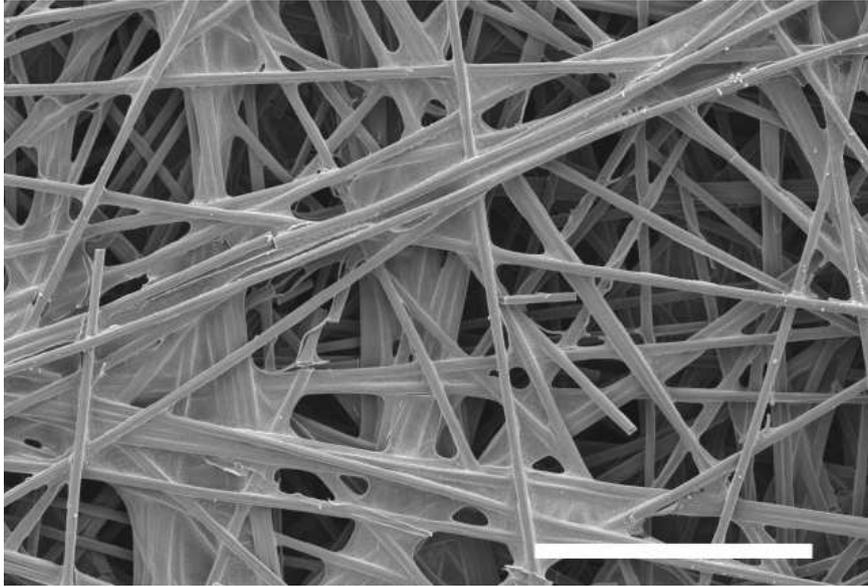
Figure 1.2: SEM image of a Toray TGP-H-060 GDL (length bar represents 200 μm) [8], a GDL typically used in PEMFC.

e.g. the porosity which is the ratio between the volume of the void and the total volume

$$\epsilon = \frac{V_{void}}{V_{total}} = \frac{V_{void}}{V_{void} + V_{solid}}. \tag{1.3}$$

The reference diffusivity chosen to be self diffusion coefficient of the species in cylindrical pores [5]. Given this definition, the formation factor is a dimensionless transport coefficient incorporating the microscopic structure of the material. There are numerous models in previous attempts to formulate a formation factor for porous media and obtain an quantitative formula considering the structure parameters. A few models are summarized in Tab. 1.1, however, we do not understand the theoretical relationship between the structure parameters and the formation factor [13]. The physics in porous media is still an unsolved problem, hence the existence of all the different model approaches. Zamel et. al. [4] investigated the diffusion coefficient for various GDLs, and found that existing models overestimated the effective diffusivity.

Legend in figure:
- Carman-Kozeny 1927, $f(\epsilon) = \epsilon/4$
- Bruggeman factor 1935, $f(\epsilon) = \epsilon^{1.5}$
- Neale and Nader, 1973, $f(\epsilon) = \frac{2\epsilon}{3-\epsilon}$
- Tomadakis factor 1993, $f(\epsilon) = \epsilon\left(\frac{\epsilon - 0.037}{1 - 0.037}\right)^{0.661}$
- Mezedur 2002, $f(\epsilon) = 1 - (1-\epsilon)^{0.46}$
- Zamel et al. 2009 Experimental data

Axis labels: Formation factor, $f(\epsilon) = D_{eff}/D_{ref}$ (vertical); Porosity (ϵ) (horizontal)
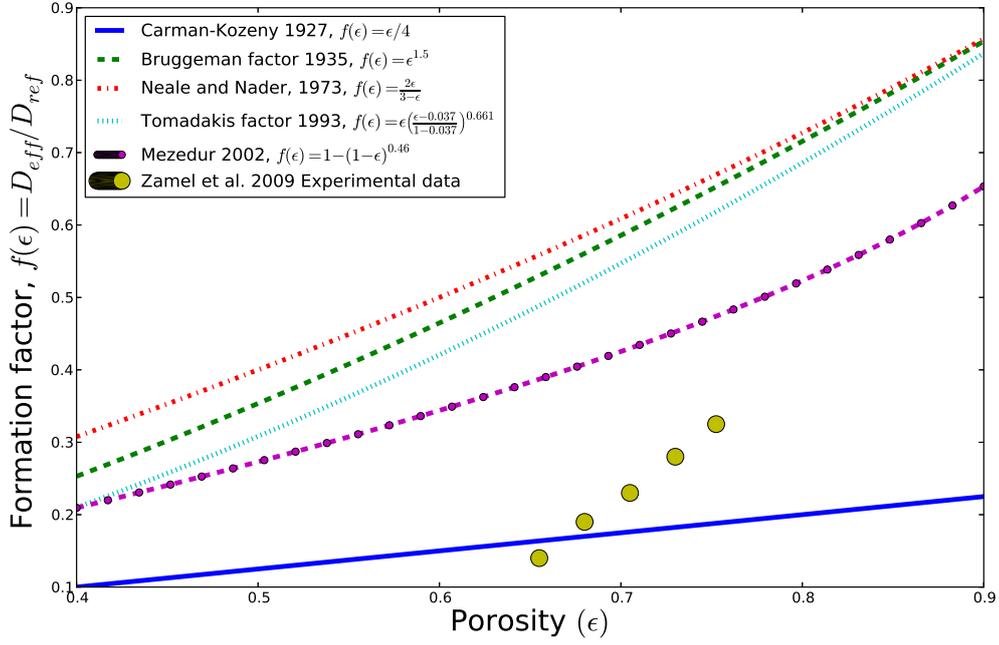
Figure 1.3: Comparison of models for the effective diffusivity against the porosity, the void fraction of the material.

Model	Formation factor (f)	Method	Year
Carman, Kozeny [11]	$\epsilon/\tau,\ \tau \sim 4$	Hypothetical path length point to point.	1927
Bruggeman [10]	$\epsilon^{1.5}$	Empirical results.	1935
Neale, Nader [12]	$2\epsilon/(3-\epsilon).$	Isotropic medium of spherical particles.	1973
Tomadakis [5]	$\epsilon_0 \left(\frac{\epsilon - \epsilon_p}{1 - \epsilon_p}\right)^{\alpha}$	Percolation theory for random fibrous media. α_0 and ϵ_0 are model parameters.	1993
Mezedur [14]	$(1 - (1-\epsilon)^{0.46})$	Two dimensional ordered and random lattice networks	2002

Table 1.1: Table of models for calculating the effective diffusivity in porous media. τ is the tortuosity or diffusional path length to be travelled to cross a region with certain thickness.

1.2 Transport Phenomena

Diffusional transport phenomena in porous media is described by the diffusion equation (Fick's Law),

$$\frac{\partial c_A(\mathbf{r},t)}{\partial t} = \nabla[D_A \nabla c_A(\mathbf{r},t)], \tag{1.4}$$

where $c_A(\vec{r},t)$ is the concentration of species A, $\mathbf{r}$ is the position vector, t is the time, and D is the diffusivity tensor for species A. In the most general case, the diffusivity tensor can vary spatially, on the concentration, in time and on the direction depending on the domain. Diffusion in static domains such as with porous media, the diffusivity tensor will not have a temporal dependence, and for diffusion in statistically homogeneous media, the diffusivity tensor becomes constant is all directions, i.e. ($\nabla D = 0$). In statistically homogeneous media, the equation above can be written as,

$$\frac{\partial c}{\partial t} = D_0 \nabla^2 c, \tag{1.5}$$

where D_0 is the reference diffusivity in equation (1.4). For further notice, we shall refer the macroscopic diffusion coefficient in porous domain as the effective diffusivity. To calculate a value for the diffusion coefficient, there are several methods applicable. It is possible to formulate the problem as a nonlinear least-squares problem [15]. The author of this study chose random walk simulations [5]. The reason to use random walk simulation is the flexibility material structures that can be used, which is well suited for scanned image data. Also, there is no assumption in the shape of the diffusion coefficient as well.

1.2.1 Solution of the Diffusion Equation

As mentioned, there are no analytically solutions to the diffusion equation in complex media. However, analytical solutions exists for simple domains. A solution to the diffusion equation in one dimension for free space will be given, and the solution method is analogue to higher dimensions.

First, we require the solution to vanish in infinity, i.e. $c \to 0$ when $x \to \pm\infty$. Then the fourier transform of the diffusion equation (1.5) yields,

$$\frac{\partial \hat{c}(\xi,t)}{\partial t} = D_x \int_{-\infty}^{\infty} \frac{\partial^2 c(x,t)}{\partial x^2} e^{-ix\xi} \mathrm{d}x, \tag{1.6}$$

which is an ordinary differential equation in t,

$$\frac{\partial \hat{c}(\xi,t)}{\partial t} = -D_x \xi^2 \hat{c}(\xi,t), \tag{1.7}$$

with the solution,

$$\hat{c}(\xi,t) = \hat{c}(\xi,0) e^{-D_x \xi^2 t},$$

where the function $\hat{c}(\xi,0)$ is the fourier transform of the initial conditions. To obtain an expression for the concentration, we apply the inverse fourier transform on the above expression and readily get:

$$c(x,t) = \frac{1}{2\pi} \int_{-\infty}^{\infty} \int_{-\infty}^{\infty} c(x',0)e^{-D_x\xi^2 t + i\xi(x-x')}\mathrm{d}x'\mathrm{d}\xi.$$

We proceed by solving the integral in ξ, using Eulers formula $e^{ix} = \cos x + i \sin x$, and the final expression for the solution to the diffusion equation in one dimension is:

$$c(x,t) = \frac{1}{\sqrt{4\pi D_x t}} \int_{-\infty}^{\infty} c(x',0)e^{-(x-x')^2/4D_x t}\mathrm{d}x. \tag{1.8}$$

We note that this expression is the convolution with a Gaussian function and the initial conditions, which says that the transient behaviour of the solution can be interpreted as particles "spread out" over time. If all the particles are positioned at x_0 at $t = 0$, which can be represented by setting the initial conditions to a delta function,

$$c(x,0) = \delta(x - x_0),$$

the resulting time evolution of the concentration distribution is,

$$c(x,t) = \frac{1}{\sqrt{4\pi D_x t}}e^{-(x-x_0)^2/4D_x t}. \tag{1.9}$$

Any type of initial condition can be expanded into a series of delta functions, hence the solution to the diffusion equation will be a superposition to the equation above.

In order to use random walk simulations, we need to know statistical properties of the diffusion equation, and in particular a statistical measurement how to relate the diffusion coefficient to the random motion of particles. Such a measurement is the Mean Square Displacement (MSD), and can be found from the diffusion equation given simple geometries where analytical solutions exist.

To calculate the MSD given an analytical solution, we can interpret the expression

$$p(\mathbf{r},t) = \frac{c(\mathbf{r},t)}{C},$$

as the distribution of finding a particle at point $\mathbf{r}$ and time t, where C is the total number of particles. Hence, the expectation value of x^2 yields,

$$\langle x^2 \rangle = \int_{-\infty}^{\infty} x^2 p(x,t)\mathrm{d}x = \frac{\int_{-\infty}^{\infty} x^2 c(x,t)\mathrm{d}x}{\int_{-\infty}^{\infty} c(x,t)\mathrm{d}x} = 2D_x t.$$

Similar results are obtained for y,z, i.e. $\langle y^2 \rangle = 2D_y t$ and $\langle z^2 \rangle = 2D_z t$. Then the total mean square displacement can be expressed, assuming isotropic conditions, i.e $D_y = D_x = D_z$,

$$\langle r^2 \rangle = \langle x^2 + y^2 + z^2 \rangle = \langle x^2 \rangle + \langle y^2 \rangle + \langle z^2 \rangle = 6Dt,$$
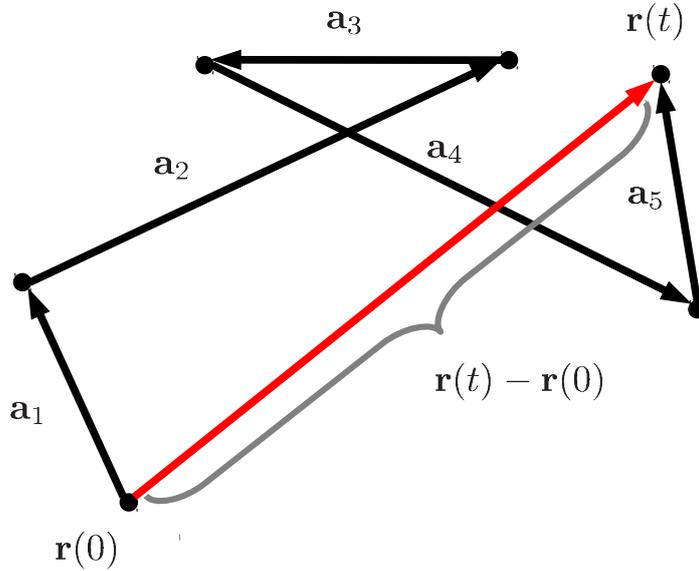
Figure 1.4: Schematic figure of a random walk.

which is the relation between MSD and the diffusion constant. If the particle starts at $\mathbf{r}(0)$, the expression yields,

$$\langle (\mathbf{r}(0) - \mathbf{r}(t))^2 \rangle = 6Dt. \tag{1.10}$$

This equation means that the MSD is proportional to the diffusion coefficient. With this statistical measurement, we can estimate the effective diffusivity of complex geometries. In the next section, we establish the relation between the MSD from a discrete random walk to the diffusion coefficient.

1.3 Discrete Random Walk

Random walk simulations have been used extensively in many fields, e.g. chemistry, economics, to investigate stochastic processes [16]. Diffusion is a stochastic process and can be well described by a random walk. The terms walker and particle will be used interchangeably. The goal of the random walk is to mimic the behaviour of gas particles in porous media. From the discrete random walk in a domain, the obtained MSD gives the diffusion coefficient.

A schematic representation of a random walk, starting at $\mathbf{r}(0)$ and ending at $\mathbf{r}(t)$ is shown in Fig. 1.4. Setting $\mathbf{r}(0) = 0$, the displacement of a random walker is expressed

as the sum of the individual steps,

$$\mathbf{r} = \sum_{i=0}^{N} \mathbf{a}_i.$$

Then the expectation value of the total displacement is,

$$\langle \mathbf{r} \rangle = \langle \sum_{i=0}^{N} \mathbf{a}_i \rangle = \sum_{i=0}^{N} \langle \mathbf{a}_i \rangle,$$

due to the linearity of the expectation value. Hence, the expected total displacement is equal to the sum of the expected value of each step. Assuming every step has the same distribution, the individual steps can be described by the joint distribution, $f(a, \mathbf{n})$, with the random variables: $\mathbf{n}$ for the direction and a for the step length. Assuming the direction and length are statistically independent, the joint distribution can be separated into two distributions,

$$f(a, \mathbf{n}) = g(a)h(\mathbf{n}), \tag{1.11}$$

one for the step direction and one for the step length. Hence, we can write the step as $\mathbf{a} = a \cdot \mathbf{n}(\theta, \phi)$, where $\mathbf{n}(\theta, \phi)$ is a dimensionless unit vector with the angles $\theta \in [0, \pi]$ and $\phi \in [0, 2\pi]$ defined by spherical coordinates.

For a random walk in free space, there will be no bias in which direction a walker can go. Hence, $h(\mathbf{n})$ will have an uniform distribution over the interval for the angles θ, ϕ, and the mean displacement of individual step yields,

$$\langle \mathbf{a} \rangle = \langle a \rangle \langle \mathbf{n} \rangle = \int_0^{\infty} ag(a)\mathrm{d}a \int_S \mathbf{n} h(\mathbf{n})\mathrm{d}\Omega = 0,$$

where the domain S is the boundary of a unit sphere. Because an odd function is integrated over a symmetric interval, the latter integral is zero. Hence, the total mean displacement is equal to zero.

The mean square displacement can now be calculated for free space, or the second moment of the total displacement with the joint distribution (1.11),

$$\langle \mathbf{r}^2 \rangle = N \langle a^2 \rangle + \sum_{i,j=0}^{N} \sum_{i \neq j}^{N} \langle \mathbf{a}_i \cdot \mathbf{a}_j \rangle \tag{1.12}$$

and because the steps are statistically independent, the cross terms $(i \neq j)$ can be written as

$$\sum_{i,j=0}^{N} \sum_{i \neq j}^{N} \langle \mathbf{a}_i \cdot \mathbf{a}_j \rangle = \langle a \rangle^2 \underbrace{\sum_{i,j=0}^{N} \sum_{i \neq j}^{N} \langle \mathbf{n}_i \rangle \cdot \langle \mathbf{n}_j \rangle}_{=0} = 0.$$

Finally for free diffusion, the mean square displacement is proportional to the number of steps taken by the walkers starting at $\mathbf{r}(0)$,

$$\langle(\mathbf{r}(N) - \mathbf{r}(0))^2\rangle = N\langle a^2\rangle, \tag{1.13}$$

which holds for all dimensions. Equating this equation with the equation (1.10), an expression for the effective diffusivity is obtained as a function of the number of steps a random walker takes.

2

Random Walk Method

In this section, the methodology for the random walk simulation is described. The goal is to validate the random walk simulations in domains derived from previous studies of Tomadakis [17], and then obtain a program to perform random walk simulations in scanned images of GDL. First, the method for generation of the validation domain will be explained, and secondly the random walk procedure.

2.1   Validation Domain

GDLs consists mainly of fibres, which can be modelled as cylinders. Tomadakis [17] performed random walk simulations in a domain built up of cylinders, defined by a random point, random direction and a radius. Hence it is reasonable to validate the random walk simulations against the work of Tomadakis [17]. In this report, however, the domain of simulation will consist of a discrete grid, which will be transferable to the scanned images of GDLs. Cylinders will be referred as fibres.

First, the algorithm used by Tomadakis [17] for generation of random fibres was performed, followed by a scheme to render the fibres discrete. In order to simulate different porous structures, random fibres are grouped into three different categories: unidirectional, bidirectional and tridirectional, representing fibers oriented in one, two and three dimensions respectively. The different structures are depicted in Fig. 2.1. In order to obtain isotropic conditions for the cylinders, the construction of fibres for the unit cube was carried out by a μ randomness scheme. This procedure ensures that the calculated diffusion coefficient will not have a spatial dependence [17]. Details about the different randomness mechanisms are described in Appendix B.

To obtain μ randomness for the fibres in the unit cube with edge length $a = 1$, one has to sample uniformly distributed fibres from an infinite plane and select the fibres that intersect the unit cube. In the code however, a sufficiently big square plane with side b was chosen ($b = 100$). The plane can be located anywhere in space, but for
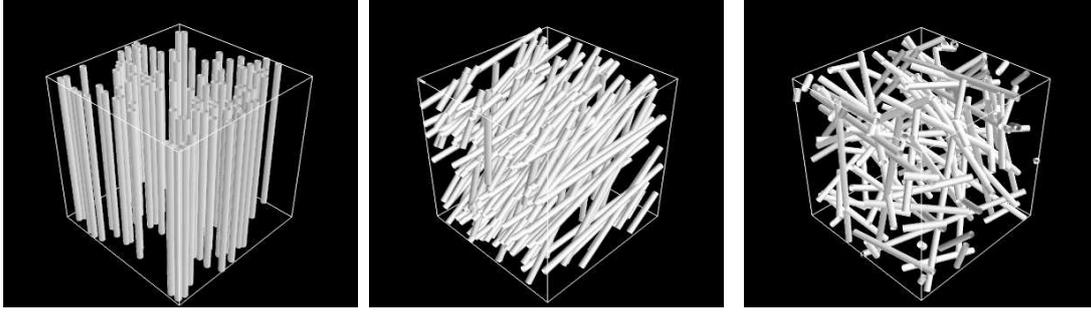
(a) Unidirectional fibres.   (b) Bidirectional fibres.   (c) Tridirectional fibres.

Figure 2.1: The different fibre structure used in the random walk simulation (porosity $\epsilon = 0.9$).

simplicity was the plane placed at $z = 0$ and the cube was placed at origo. To obtain the μ randomness, the polar angle θ had to be sampled based on the cosine law [18] and the azimuthal angle ϕ was sampled between $[0, 2\pi]$ for each fibre. The distribution for the polar angle is

$$f(\theta)\mathrm{d}\theta = 2\sin\theta\cos\theta\mathrm{d}\theta = d(cos^2),$$

hence uniform distribution of $\cos^2\theta$. Derivation for the polar angle distribution is found in section B.1. Using two uniformly distributed variables between [0,1], ξ_1 and ξ_2, the resulting directions for the fibres are:

$$\cos\theta = \sqrt{\xi_1} \tag{2.1a}$$
$$\phi = 2\pi\xi_2 \tag{2.1b}$$
$$v_x = \sin\theta\cos\phi \tag{2.1c}$$
$$v_y = \sin\theta\sin\phi \tag{2.1d}$$
$$v_z = \cos\theta \tag{2.1e}$$

Based on probability arguments, it is possible to calculate the porosity ϵ, defined in equation (1.3), for a domain of random fibres [17]. The formula for the number of traces of fibres per unit area on face of the unit cube is,

$$N_f = \frac{1}{\bar{l}d}\frac{-\log\epsilon}{\pi r^2}, \tag{2.2}$$

where d denotes the directionality of the fibres ($d = 1,2,3$), $\bar{l}$ is the mean length of fibres inside the unit cube and r is the radius of the fibres. For unidirectional fibres $\bar{l} = 1$, and for bidirectional and tridirectional structures it can be shown that $\bar{l} = \pi A/C$ [18] and $\bar{l} = 4V/S$ [19] respectively, where V denotes the cube volume , S the surface of the cube and C the circumference of one face of the unit cube. Sampling fibres from a plane with $b = 100$ proved sufficient to obtain a number of traces on each face of the cube to be close enough to N_f.

(a) Unidirectional fibres.   **(b)** Bidirectional fibres.   **(c)** Tridirectional.
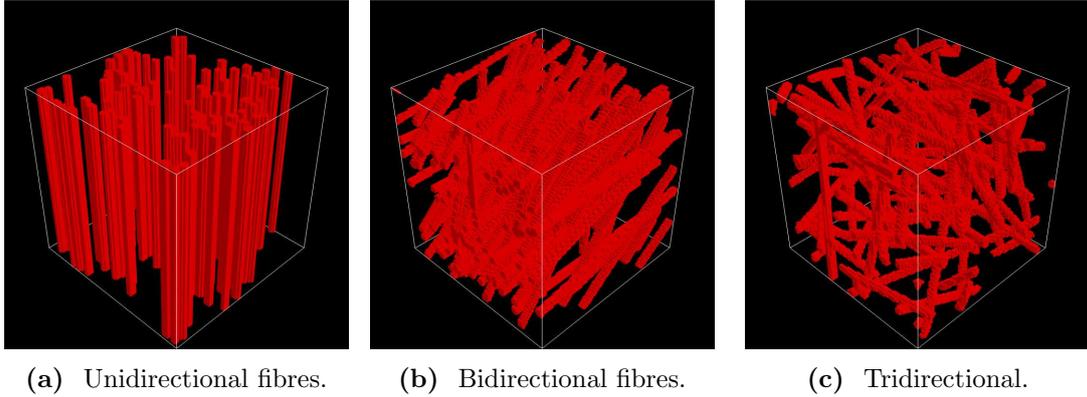
Figure 2.2: The different fibre structure used in the random walk simulation (porosity $\epsilon = 0.9$), discretized domain.

To render the fibres discrete, a lattice with N_g^3 points was tested for overlap with the fibres defined by point, direction and radius. Then each lattice point defined a voxel in an uniform grid, where the voxel was either void or solid. The ratio between the unit cube length and the radius was chosen to $r/a = 0.02$, which guarantees statistically acceptable samples of the structure [17]. Figures of the discretized domain is shown in Fig. 2.2.

Periodic boundary conditions were used in order to obtain a large simulation space. In a symmetric unit cell, the particle leaving the cube can be reintroduced at the opposite face of the cube. A unit cell with random structures however, cannot be periodically repeated [17]. For instance, if the particle crosses the boundary at $x = 1$, it cannot reappear at $x = 0$ if that voxel is occupied by a fibre. The solution is to place a mirrored image of the unit cell next to the unit cell. The periodic cell will be 2, 4, 8 unit cells in one, two, three dimensions respectively.

2.2   Particle Trajectories

The effective diffusivity can be as mentioned in section 1.2.1 calculated from the mean square displacement of random walkers. Random walks are done over a large number of walkers, and then an average for the displacement squared can be calculated. The behaviour of the walkers, is as mentioned to characterize the behaviour of gas particles in porous media. The algorithm for the random walk is similar to the construction of random fibres described in previous section 2.1. First the start position $r(0)$ of the walkers are uniformly distributed inside the domain. If the start position is inside a solid voxel, then the position is rejected and a new position is sampled. The direction of walkers in void is sampled according to the distribution described in section 1.3. The polar angle θ, $[0,\pi]$, and the azimuthal angle ϕ, $[0,2\pi]$, are distributed so that corresponding points on the boundary of a sphere are uniformly distributed. Performing a probability integral transform on the solid angle, the angles can be expressed with two

uniformly distributed variables between [0,1], ξ_1 and ξ_2, and the resulting equations are,

$$\cos\theta = 2\xi_1 - 1 \tag{2.3a}$$

$$\phi = 2\pi\xi_2 \tag{2.3b}$$

$$w_x = \sin\theta\cos\phi \tag{2.3c}$$

$$w_y = \sin\theta\sin\phi \tag{2.3d}$$

$$w_z = \cos\theta \tag{2.3e}$$

where u_f, v_f, w_f are the directional cosines.

To account for the inter-particle collisions in the gas, each walker is assigned a step length λ from an exponential distribution parametrized by a mean free path $\bar{\lambda}$,

$$f_{\bar{\lambda}}(\lambda) = \frac{1}{\bar{\lambda}}e^{-\lambda/\bar{\lambda}}. \tag{2.4}$$

The derivation of this exponential distribution is done in appendix A. The mean free path is determined by the macroscopic conditions and the diffusing particles,

$$\lambda = \frac{k_b T}{P\sqrt{2}\pi d_g^2}, \tag{2.5}$$

where k_b is the boltzmann constant, T the temperature, P the pressure and d_g the diameter of the diffusing particles. According to Tomdakis [17], the exponential distribution is valid for particles with constant velocity. It is assumed that the particles are hard spheres and elastic collisions occur between particles. After an inter-particle collision, the walker is assigned new random directions according to (2.3). This is not valid for single collisions between between particles, because momentum is conserved, and the directions after inter-particle collisions is well defined. However, after sufficiently many inter-particle collisions, the angular distribution after will converge to normal distribution, the same distribution for collisions in free diffusion, according to the law of large numbers. This assumption is similar to the assumptions in the Drude Model [20] for electron collisions.

Given an assigned step length, the walker advances along its random direction. If the walker collides with a voxel that is a solid (fibre), before it could travel its assigned length, the walker stops at the intersection between the walker trajectory (a line) and the colliding side of the voxel (a plane). The surface of the fibres on a microscopic scale is rough, and a specular collision for the gas particle is highly unlikely. This assumption has been experimentally verified by Bird [21].

At the collision point the walker is assigned a new sampled step length and a random direction away from voxel. With the same argument as for the distribution of fibres in space, the new direction after collision shall not have any bias, hence, isotropic conditions. This is achieved by giving walker directions according to the equations (2.1). All collision surfaces in the discretized domain, will have normals parallel and antiparallel to the x,y,z axes. If the direction is sampled with z as normal, then the direction is rotated to be parallel with the normal of the plane of collision.
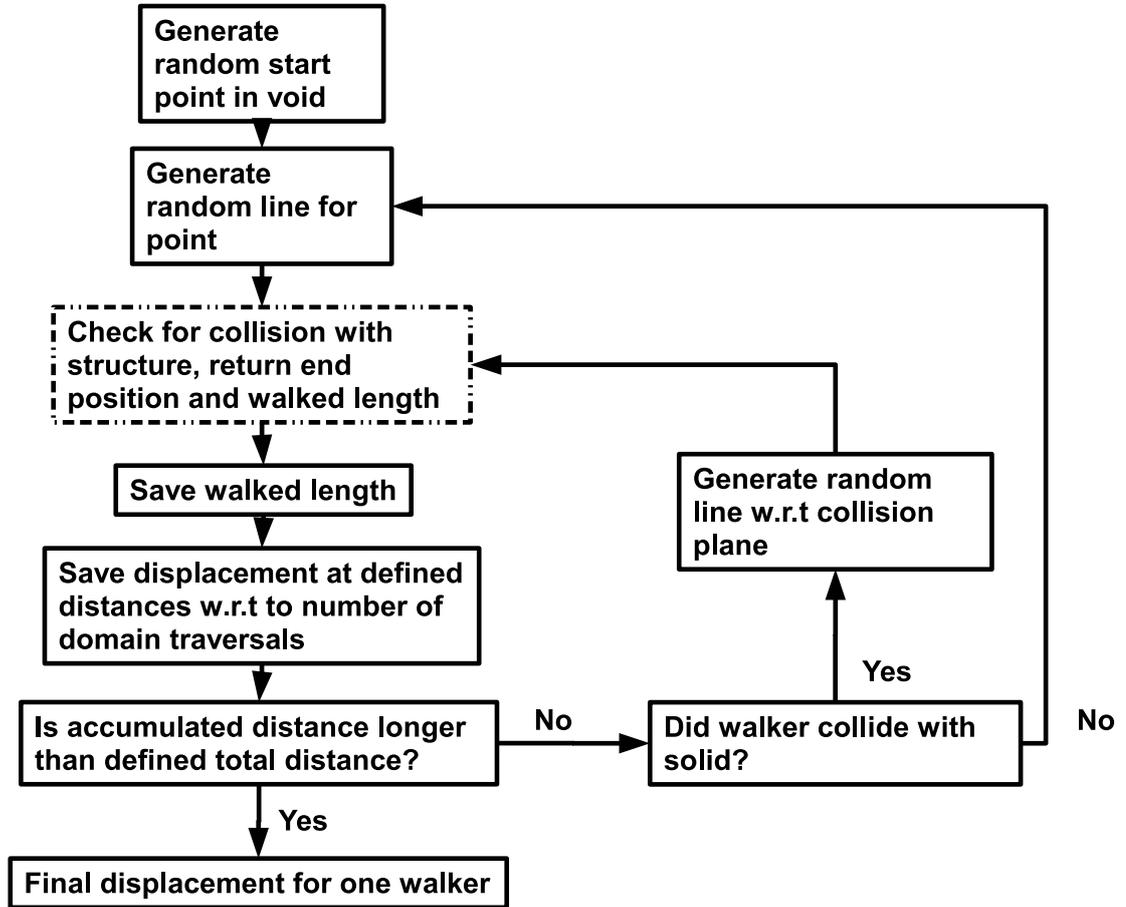
Figure 2.3: Flowchart for one walk. The dashed box, the check for collision procedure was the most computationally expensive one.

2.3 Algorithm

The algorithm for one walk described in previous section was implemented using *Python* according to the flowchart shown in Fig. 2.3. *Python* was chosen due to it's short development time. The algorithm starts with generating a start position for the walker, the algorithm continues with generating a random straight line the walker has to walk. Then a collision detection will determine whenever the walker collided or not the with structure. After each straight step walked, the displacement was saved while accounting for the boundary conditions,

$$x_{i+1} \quad = \quad x_i + (-1)^{n_x(i)} w_x(i) \tag{2.6a}$$

$$y_{i+1} \quad = \quad y_i + (-1)^{n_y(i)} w_y(i) \tag{2.6b}$$

$$z_{i+1} \quad = \quad z_i + (-1)^{n_z(i)} w_z(i), \tag{2.6c}$$

where $n_j(i)$ is the number of specular reflections the walker has done on the boundary. The walker advances until a predefined distance has been accumulated.

The procedure for collision detection between structure and walker was the function which required most time during the simulation. To calculate the intersecting grid cells of a walker trajectory, we use the fact that a line segment in a uniform grid has constant distance between grid cell boundaries. An efficient algorithm is described by Ericson [22]. The walker has line segment to travel,

$$\mathbf{p}_1 = \mathbf{p}_0 + \mathbf{w} t_w,$$

where $\mathbf{p}_0$ is the start position, $\mathbf{p}_1$ the end position, $\mathbf{w}$ the direction (unit length) and t_w is the length sampled from the exponential distribution (2.4). First, calculate which start cell, i_l, $l = x,y,z$, the walker occupies at position $\mathbf{p}_0$. From the start cell calculate the distances along the walker direction $\mathbf{w}$ to the closest x,y,z boundary of the adjacent grid cells, t_{l0}. Then calculate the distance between the boundaries of the grid cells,

$$\Delta t_l = \frac{M}{w_l},$$

where M is the grid cell length and w_l the components of the direction of the walker. The the walk consists of in each step comparing the t_l values,

$$t_l = t_{l0} + n_l \Delta t_l, \tag{2.7}$$

where n_l is the number of times t_l was the smallest value among $l = x,y,z$. When the component l has the smallest value, it means adding 1 or -1 to i_l, and then check the grid cell at i_x,i_y,i_z. The next cell to visit is determine by the updated values of (2.7).

This collision detection imposes a significant amount of array elements, representing the structure, to be accessed, and it is the reason why it was the most computationally expensive function of the program. To speed up calculations, this part of the program was converted into C using *Cython* [23], because C has more efficient memory allocation and memory accessing than *Python*.

As mentioned, periodic boundary conditions with two mirrored unit cells are applied. This is equivalent to a specular reflection when the walker hits the boundary. By keeping global and local coordinates in the unit cell for the walker, the total displacement can be calculated. It is important to know in which cell the walker is located, because a direction sampled in the unit cell after collision with structure has the component parallel to the normal of the collision plane reversed.

The simulation program was parallized using Message Passing Interface (MPI), and the schematic flowchart for the implementation is shown in Fig. 2.5. The library used to
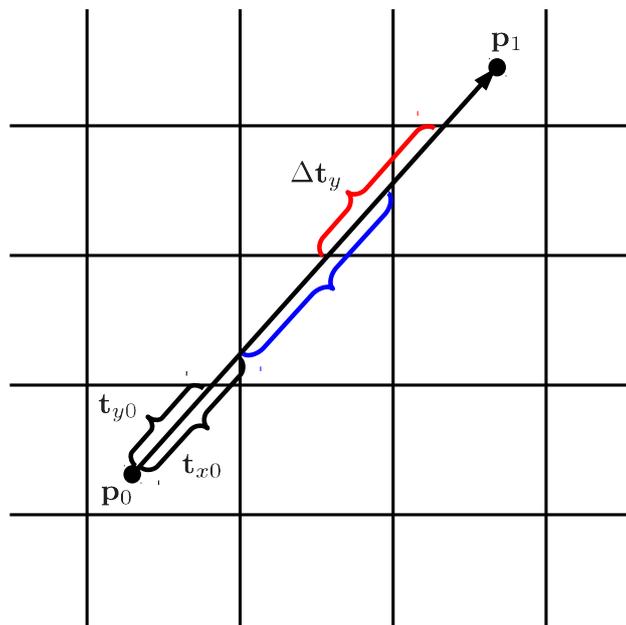
Figure 2.4: Schematic for collision detection between walker and the structure.
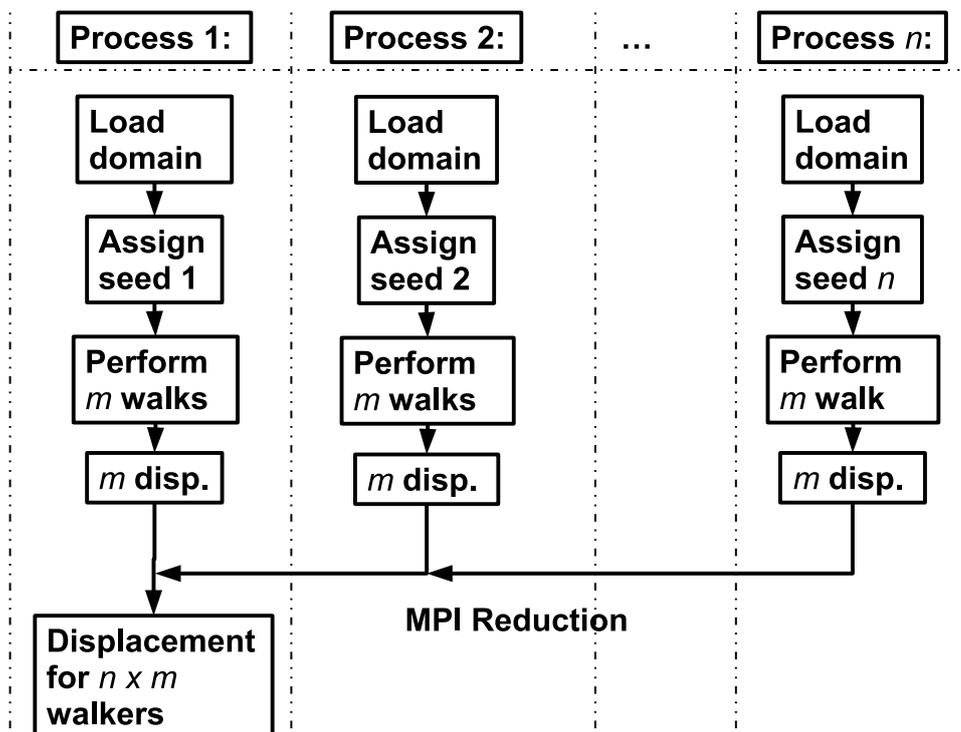
Figure 2.5: Flowchart for MPI operations.

implement the MPI interface was *mpi4py*. In this implementation, all processes load an individual copy of the domain for collision detection, making the program inefficient in terms of memory usage. To obtain random numbers for all processes, different seeds for the processes were used. In this simulation program, the rank of the process was used as the individual process seed. If different seed is not provided, then the walks on each process would be identical to each other.

3

Results and Discussion

To illustrate the nature of a random walk in fibrous porous media, one walk is depicted in Fig. 3.1, where the mean free path is $\lambda = 0.78$ and the walker takes 300 steps. As can be seen, the walker collides significantly with the structure when the step length is more than half the cube size.

In order to obtain a value for the effective diffusivity, the number of walkers and the length of the travel distance, $s = \langle v \rangle t$ had to be estimated. The number of walkers was chosen to be an order of magnitude larger than the number of steps done for a given travel distance, which proved sufficient. The travel distance was chosen so that the ratio between the MSD for diffusion in the structure and free diffusion converged. The relative MSD for different mean free paths are shown in Fig. 3.2. The number of walkers is $2.4 \cdot 10^5$ and the number of grid cells is 128^3. The porosity calculated by counting cells that are void and solid is 0.606, close to the value of 0.6 used to parametrise the number of fibres in the domain using the equation (2.2).

In the ratio between MSD in fibres and free diffusion the simulation artefacts cancel. For very short travel distances, the ratio is almost one, meaning that the walkers have not yet "felt" the presence of the structure. As the travel distance increases, the walkers in the structure collides and the MSD decreases compared to free diffusion, and after a sufficiently long travel distance the MSD in the structures flattens out. The simulation with longer mean free paths have a lower relative MSD, because the walkers have a higher probability of colliding with the fibres on each step compared to free diffusion.

The results for the simulation was validated against the simple Bosanquet formula (series addition of diffusivities),

$$\frac{1}{D_{trans}} = \frac{1}{D_{bulk}} + \frac{1}{D_{knudsen}},\tag{3.1}$$

commonly used to calculate the effective diffusivity of porous media, and which Tomdakis [17] found a good agreement with his results. The diffusivities D_{trans}, D_{bulk} and
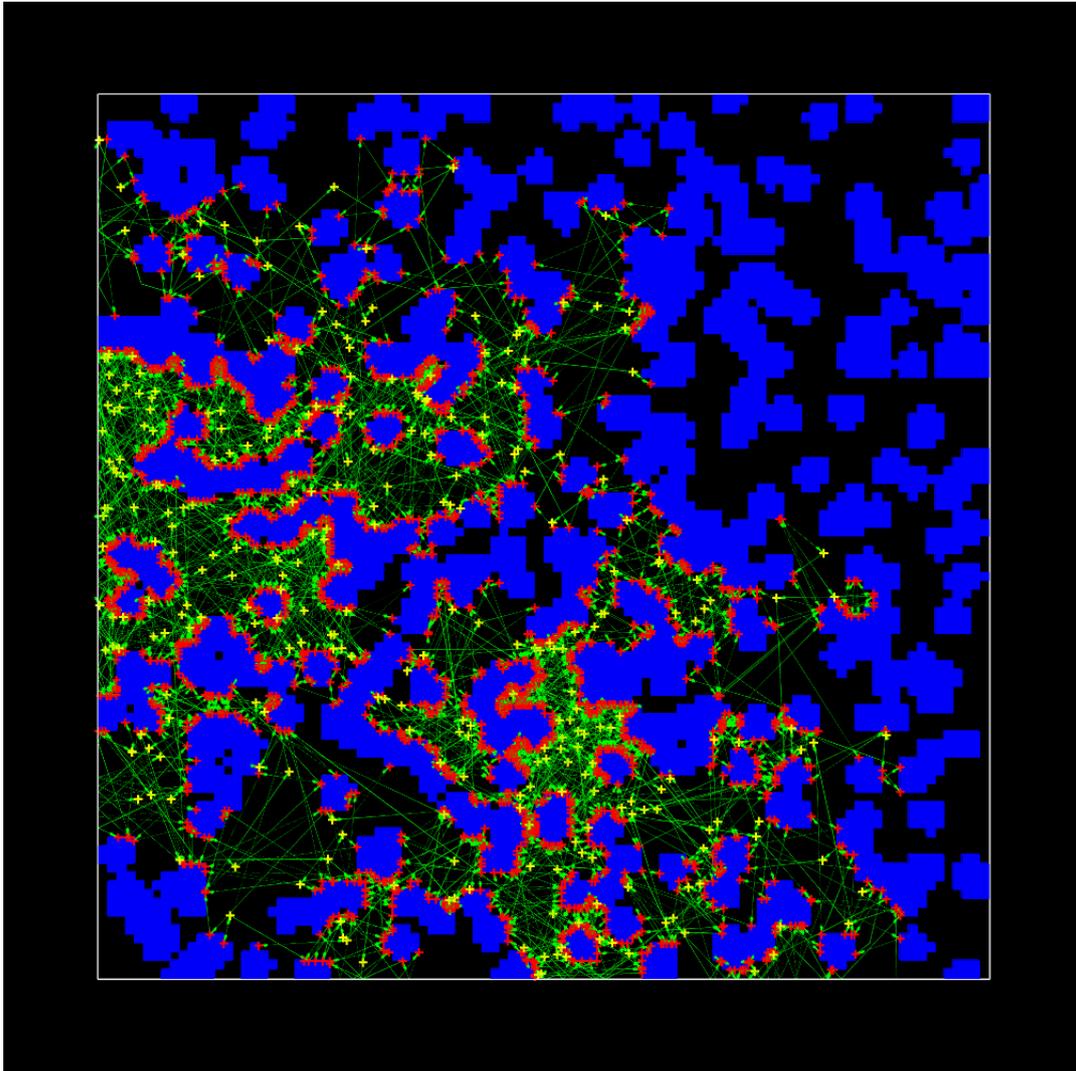
Figure 3.1: One walk in unidirectional fibres, $\epsilon = 0.6$, $kn = 10$ and total length walked is $300\bar{\lambda}$. Red cross and yellow cross indicates collision with fibre and particle collision respectively.
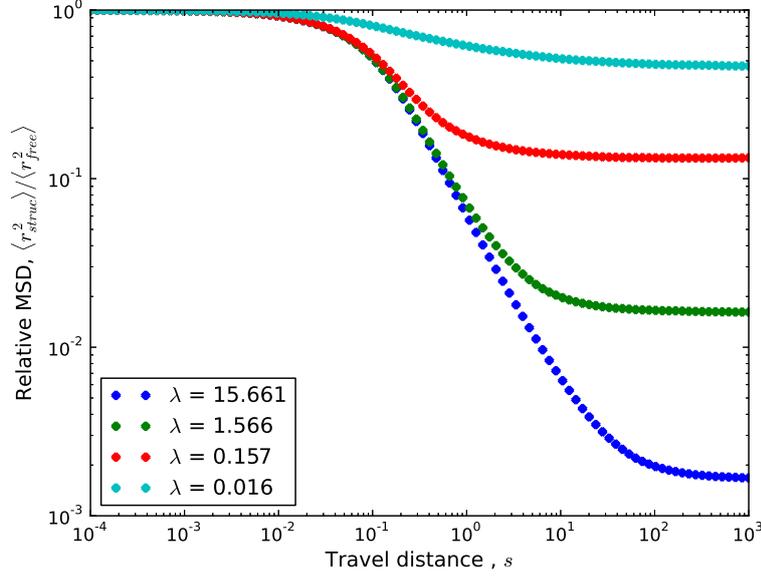
Figure 3.2: The ratio between the MSD in fibres and the MSD for free diffusion plotted against the travel distance. All simulations has $N_{walks} = 2.4 \cdot 10^5$, except $\lambda = 0.016$ which has $N_{walks} = 4 \cdot 10^5$. The porosity is $\epsilon = 0.6$, 128^3 grid cells and the simulation is performed in tridirectional fibres.

$D_{knudsen}$, are the diffusivities in the transition regime, bulk regime and Knudsen regime, respectively. These regimes are categorized by the Knudsen number,

$$Kn = \frac{\lambda}{d}, \tag{3.2}$$

where λ is the mean free path of the particles and d is the characteristic pore size of the porous media. Diffusion in the bulk regime has a low knudsen number $Kn < 0.01$, which means that particles are colliding more with other particles than with the structure. The knudsen regime describes the opposite, a high knudsen number $Kn > 100$, and particles collides much more with the structure than with other walkers. The transition regime is then the conditions between the bulk and the knudsen regime, $0.01 < Kn < 100$.

The diffusivities for the bulk and the knudsen regime is,

$$D_{bulk} = \frac{1}{3}\langle v\rangle\lambda \tag{3.3a}$$

$$D_{knudsen} = \frac{1}{3}\langle v\rangle d, \tag{3.3b}$$

where $\langle v\rangle$ is the mean velocity of the particles. Then using the definition for the knudsen number and the equations above, the Bosanquet formula can be rewritten as
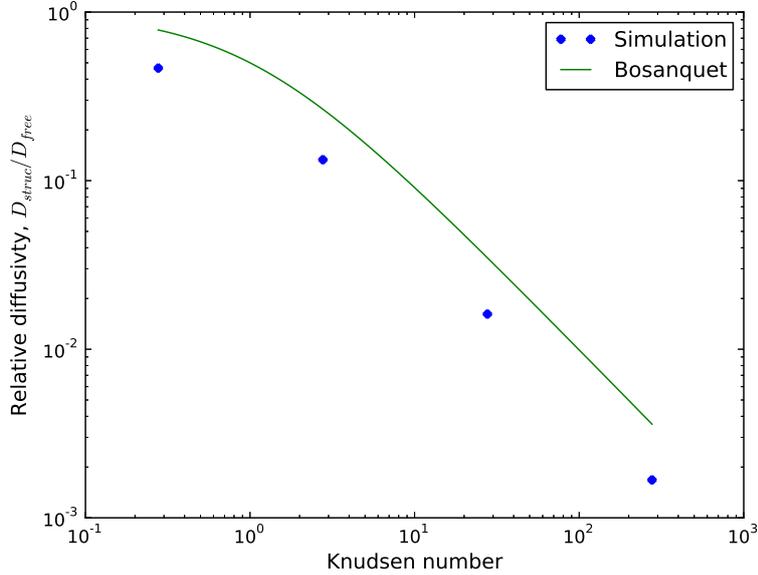
Figure 3.3: The relative diffusivity plotted against the knudsen number. The knudsen number is estimated with equation (3.5).

$$D_{trans} = \frac{D_{bulk}}{1 + Kn}, \tag{3.4}$$

which is plotted in Fig. 3.3. The knudsen number for the simulations is estimated from the formula [17]

$$\frac{C_{wm}}{C_{mm}} = Kn, \tag{3.5}$$

where C_{wm} is the number of molecule-wall collisions and C_{mm} is the particle-particle collisions. In the figure, it is seen that the relative diffusivity is smaller than the diffusivity described by equation (3.1). The relative error is ~ 0.5 compared to the Bosanquet formula for all simulation points. A plausible explanation to this discrepancy is the grid size. The domain used by Tomadakis [17], is defined by continuous fibres, whereas the fibres in the simulation represented in Fig. 3.3 are discrete. However, at $\epsilon = 0.6$ the relative error in porosity, between the discrete domain and the continuous domain, is $\sim 2 \cdot 10^{-4}$, which suggest that other systematic errors could be present.

4

Conclusion

The goal of the thesis, to obtain a simulation program adapted for scanned images of porous material, is well under construction. The results in figures 3.2 and 3.3 suggest an expected behaviour from the random walk simulations. The objective of validating the simulation with the work of Tomadakis, is yet to be done. The discrepancy between the Bosanquet formula and the results suggests that there may be a systematic error in the simulation. A plausible phenomenon could be the discretization degree, and changing the number of grid cells would give more insight of the discretization effect. However, the Bosanquet formula does not need to be correct. For instance, Baten [24] reported that the formula overestimate the effective diffusivity for low pore concentrations in mesopores.

Further, what needs to be done is additional testing of the program, investigating different porosities and structures of fibres. When the program can replicate the work of Tomadakis, it is possible to perform studies on scanned materials. A more sophisticated error analysis would also contribute to the validity of the results.

In order to increase the simulation speed, a suggestion would be to use a compiled language. The program now is written in *Python*, an interpreted language, with critical parts of the program converted into *C*. An interpreted language have difficulties of reaching the speed of a compiled language, where it is possible to have efficient memory allocation and variable declaration. However, the development time in *Python* is in general faster than *C*, but only to the degree of having an working algorithm qualitatively. To ensure a quantitatively working program, the simulation speed needs to increase for debugging purposes. With the algorithm done in *Python*, the transition to *C* would be easier.

To be able to perform the simulation on large domains, a more sophisticated parallel program is needed. Currently, every processor has its own input data for the structure, and it is not possible to use domains bigger than the memory of one processor. Because the program only reads from the structure, the memory usage would decrease if the

processors could share the memory for the domain, or to distribute different parts of the domain to the processors.

The algorithm described in section 2.2, is a general algorithm for collision detection in an uniform grid. However, depending on step length and the structure of the domain, there is significant gains in speed that can be made. By categorizing the structures into bigger objects, thus obtaining a multigrid, one can apply the concept of broad collision and narrow collision detection. This is a common approach in the scientific community, as well as in many computer games.

Bibliography

[1] J.-H. Wee, Applications of proton exchange membrane fuel cell system, Renewable and Sustainable Energy Reviews 11 (2006) 1720–1738.

[2] J. Wishart, Z. Dong, A. Secanell, Optimization of a pem fuel cell system based on empirical data and a generalized electrochemical semi-empirical model, Journal Of Power Sources 161 (2006) 1041–1055.

[3] M. M. Mench, Hydrogen Energy, Wiley-VCH, 2010, Ch. 5.

[4] N. Zamel, et. al., Experimental measurements of effective diffusion coefficient of oxygen nitrogen mixture in pem fuel cell diffusion media, Chemical Engineering Science 65 (2009) 931–937.

[5] M. M. Tomadakis, S. V. Sotirchos, Ordinary and transition regime diffusion in random fiber structures, AIChE Journal 39 (1993) 397–412.

[6] M. M. Mench, Polymer Electrolyte Fuel Cells, John Wiley & Sons, Inc., 2008, Ch. 6, pp. 285–379.
URL http://dx.doi.org/10.1002/9780470209769.ch6

[7] The department of energy hydrogen and fuel cells program plan (September 2011).

[8] A. Bazylak, Liquid water transport in fuel cell gas diffusion layers, Ph.D. thesis, University of Victoria (2008).

[9] S. Litster, N. Djilali, Transport Phenomena in Fuel Cells, WIT Press, Southampton, 2005, Ch. 5, pp. 175–213.

[10] D. A. G. Bruggeman, Berechnung verschiedener physikalischer konstanten von heterogenen substanzen. i. dielektrizitätskonstanten und leitfähigkeiten der mischkörper aus isotropen substanzen, Annalen der Physik 416 (1935) 636–664.

[11] P. Carman, Fluid flow through granular beds, Transactions, Institution of Chemical Engineers, London 15 (1937) 150–166.

[12] G. Neale, N. Epstein, W. Nader, Creeping flow relative to permeable spheres, Chemical Engineering Science 28 (1973) 1865–1874.

[13] P.-Z. Wong, Methods of the Physics of Porous Media, Academic Press, 1999.

[14] M. M. Mezedur, M. Kaviany, W. Moore, Effect of pore structure, randomness and size on effective mass diffusivity, AIChE Journal 48 (2002) 15–24.

[15] S. Wang, X. Lou, Numerical methods for the estimation of effective diffusion coefficients of 2d controlled drug delivery systems, Optimization and Engineering 11 (2010) 611–626, 10.1007/s11081-008-9069-8.
URL http://dx.doi.org/10.1007/s11081-008-9069-8

[16] N. G. V. Kampen, Stochastic Processes in Physics and Chemistry, Elsevier, Amsterdam, 1992.

[17] M. M. Tomadakis, Transport and structural properties of fiber-reinforced composites and porous media of fibrous or capillary structure, Ph.D. thesis, The University of Rochester (1993).

[18] A. Kellerer, Considerations on random traversal of convex bodies and solutions for general cylinders, Radiation Research 47 (1971) 359.

[19] R. Coleman, Random paths through convex bodies, Journal of Applied Probability 6 (1969) 430–441.

[20] N. W. Ashcroft, D. N. Mermin, Solid State Physics, 1st Edition, Thomson Learning, Toronto, 1976.

[21] G. A. Bird, Molecular gas dynamics, Clarendon Press, 1976.

[22] C. Ericson, Real-Time Collision Detection, Morgon Kaufmann Publishers, 2005.

[23] D. S. Seljebotn (Ed.), Fast numerical computations with Cython, Proceedings of the 8 th Python in Science Conference, 2009.

[24] J. M. v. B. Rajamani Krishna, Investigating the validity of the bosanquet formula for estimation of diffusivities in mesopores, Chemical Engineering Science 69 (2012) 684–688.

[25] R. D. Present, Kinetic theory of gases, New York: McGraw-Hill, 1958.

[26] F. O. Goodman, H. Y. Wachman, Dynamics of Gas-surface Scattering, Academic Press Inc, 1976.

A

Mean free path derivations

In this section, we derive the distribution of the mean free path for particles in gases, and the mean free path for particles colliding with a wall.

Mean free path

The definition of the mean fee path is the average distance between particle collisions, how far a particle travels in average before it collides with another particle. The derivation of this distribution is based on the assumption that particles are hard spheres and they collide elastically. The problem may be also defined as, the distance travelled by a particle from an arbitrary point before a collision with another particle. Hence, the probability of a collision for a particle will not depend on the history of the trajectory of the particle.

To derive the distribution, we look at the probability for a collision to happen beyond a travelled distance ξ, or complimentary that no collision occurs within distance ξ,

$$P[x|x > \xi] = F(\xi) = \int_\xi^\infty f(x)\mathrm{d}x,$$

Now look at the probability of collision in the interval $[\xi, \xi + d\xi]$. According to Present [25], the probability of collision in the specified interval is proportional $d\xi$. So we write the probability of collision in the specified interval as $\alpha d\xi$ and α is independent of ξ because the medium is homogeneous and the chance of collision is the same everywhere. In general, α depends on the particle density, pressure, particle size and speed. The probability of no collision in the interval $[\xi, \xi+d\xi]$ is then $1-\alpha d\xi$. Because the probability of collision is independent of the history of the particle, we can write the probability of no collision after distance $\xi + d\xi$ as the product of the probability at ξ and $\xi + d\xi$:

$$F(\xi)(1 - \alpha d\xi) = F(\xi + d\xi) = F(\xi) + \frac{dF}{d\xi}d\xi,$$

which gives,

$$\frac{dF}{d\xi} = -\alpha F(\xi).$$

Solving this equation with initial condition $F(0) = 1$ (probability of collision in the whole domain) yields,

$$F(\xi) = e^{-\alpha\xi}.$$

The probability of no collision in the interval $[\xi, \xi + d\xi]$ can now be expressed with the PDF,

$$f(\xi)d\xi = F(\xi) - F(\xi + d\xi) = -\frac{dF}{d\xi}d\xi,$$

which gives,

$$f(\xi) = \alpha e^{-\alpha\xi}.$$

The expectation value of the distance between collisions is,

$$\lambda = \langle\xi\rangle = \int_0^\infty \xi f(\xi)d\xi = \alpha \int_0^\infty \xi e^{-\alpha\xi}d\xi = \frac{1}{\alpha}, \tag{A.1}$$

also known as the mean free path λ. The PDF can then be written in terms of the mean free path:

$$f(\xi) = \frac{e^{-\xi/\lambda}}{\lambda}, \tag{A.2}$$

hence the exponential form of the distribution. We can readily also calculate the second moment of the exponential distribution,

$$\langle\xi^2\rangle = \int_0^\infty \xi^2 \frac{e^{-\xi/\lambda}}{\lambda}d\xi = 2\lambda^2 \tag{A.3}$$

Mean free path distribution after collision

The derivation of the mean free path distribution after collision with a wall is based on Maxwell velocity distribution arguments [26]. The situation that describes collisions with a wall, is equivalent to particles crossing an imaginary plane when considering completely elastic collisions. The goal is to find the mean free path distribution of those particles crossing that plane.

The velocity distribution of particles hitting a wall $G(v)$, is found to be the velocity distribution of the gas as whole $g(v)$, but with a weighting factor of v,

$$G \propto vg(v).$$

In analogy, for the mean free path distribution for particles colliding with a wall $L(\xi)$, the weighting factor is ξ. The mean free path distribution of the gas as whole is $l(\xi)$ (same as (A.2)). Hence, we obtain the relation

$$L(\xi) \propto \xi l(\xi).$$

To find the proportionality constant, we normalize $L(\xi)$,

$$1 = \int_0^\infty L(\xi)d\xi = C\int_0^\infty \xi l(\xi)d\xi = C\lambda,$$

where λ is the mean free path we calculated in equation (A.1). We calculate the new mean free path for particles passing the imaginary plane,

$$\lambda' = \int_0^\infty \xi L(\xi)d\xi = \frac{1}{\lambda}\int_0^\infty \xi^2 l(\xi)d\xi = 2\lambda.$$

Hence, the mean free path for particles colliding with a wall have the double mean free path than the gas as whole.

B

Randomness mechanisms

When Tomadakis[17] is building up the unit cell with random distribution of cylinders in space, the goal is to have an uniform porosity through out the unit cell. The underlying problem is how to draw chords between distinct boundary points of the unit cell, or more generally in a convex body to obtain different statistical properties. There are several ways of distributing the chords and describing their probability distributions, but the main ones are:

- μ randomness: A chord of a convex body is defined by a point and a direction in the Euclidian space. The point and the direction are from independent uniform distributions. This randomness results if the convex body is exposed to a uniform, isotropic field of straight infinite lines.

- Interior radiator randomness (I randomness). A chord is defined by a point in the interior of the convex body and a direction. The point and the direction are from independent uniform distributions.

- Surface radiator randomness (S randomness). A chord is of a convex body is defined by a point on its surface and a direction. The point and the direction are from independent uniform distributions.

B.1 Cosine Law

In this section the cosine law distribution is derived to obtain μ randomness for chords distributed in a convex body.

Consider figure B.1, where a convex body is depicted with volume V, surface area S. Then a secant is defined as the line segment y between two points on the surface as shown in the figure. Then from each end of the secants, another secant is put out. To calculate the average length of the secants, which is defined as the mean chord length ,

30
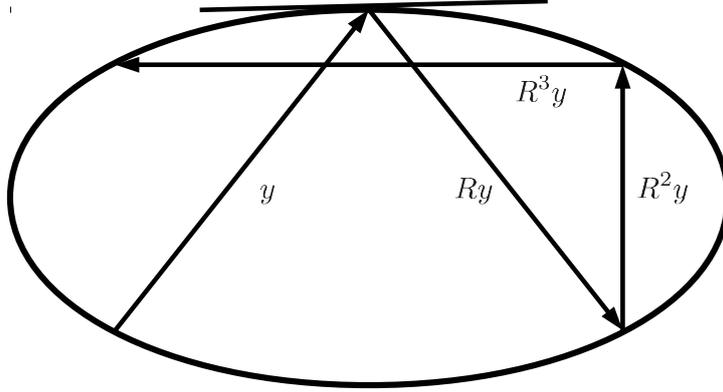
Figure B.1: Schematic figure of a lines in a convex body.
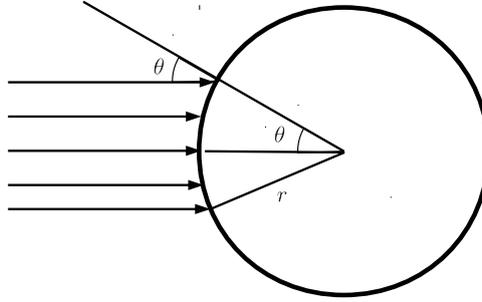
Figure B.2: Schematic figure of sphere in an unidirectional field of lines.

$$\langle l(y) \rangle = \lim_{n \to \infty} \frac{1}{n} \left[l(y) + l(Ry) + l(R^2 y) + ... + l(R^n y) \right], \tag{B.1}$$

where $l(R^n y)$ is the secant after reflection n. If this value exist, we want to make it independent of the angle of reflection, hence reflection invariant. This invariance would also rise if we put a convex body in an isotropic field of infinite lines, as described in the μ randomness description. The question arises how to put out the secants in the convex body to obtain the μ randomness.

In the μ randomness algorithm, a fix infinite plane is defined where points are uniformly distributed. These points will be the intersection of the lines and the plane. Then we want to derive the angular distribution for the angle between the normal of the fix plane and the lines.

From a surface element on a convex body, the distribution of incident angle of the line does not depend on the orientation of surface element. Considering a sphere as a convex body. One can assume a unidirectional field, because in this case all the angles will be represented on the sphere. The idea is depicted in figure B.2. The angle between the surface normal and the lines is θ, and we want to relate the angle to the cross section of the sphere. The total cross section of the sphere will be,

$$A_{tot} = \pi r^2,$$

and the cross section spanned by θ will be

$$A_1 = \pi r^2 \sin \theta.$$

The complimentary area will be,

$$A_2 = \pi r^2 - \pi r^2 \sin^2 \theta = \pi r^2 \cos^2 \theta.$$

Then the probability of the angle exceeding θ is

$$F_\mu(\theta) = A_2 / A_{tot} = \frac{\pi r^2 \cos^2 \theta}{\pi r^2} = \cos^2 \theta.$$

The probability density function is the derivative of the F_μ,

$$\frac{\partial F_\mu(\theta)}{\partial \theta} d\theta = f_\mu d\theta = 2 \sin \theta \cos \theta d\theta, 0 < \theta < \pi/2$$